Dalton Transactions

ROYAL SOCIETY OF CHEMISTRY

PAPER

View Article Online
View Journal | View Issue

Cite this: *Dalton Trans.*, 2023, **52**, 11062

A zeolitic imidazolate framework-90-based probe for fluorescent detection of mitochondrial hypochlorite in living cells and zebrafish†

Ling Zhang,‡[a] Xi Chen,‡[a] Wei-Na Wu,*[a] Xiao-Lei Zhao,[a] Yun-Chang Fan,[a] Yuan Wang,*[a] Zhi-Hong Xu,*[b,c] Ayman Nafady,[d] Abdullah M. Al-Enizi[d] and Shengqian Ma*[e]

Received 19th March 2023,
Accepted 13th July 2023

DOI: 10.1039/d3dt00829k

rsc.li/dalton

An inorganic–organic hybrid probe MP-ZIF-90 was synthesized *via* a simple condensation reaction based on the free CHO groups of zeolitic imidazolate framework-90 (ZIF-90) and 4-methyl-1-(4-(4,4,5,5-tetramethyl-1,3,2-dioxaborolan-2-yl)benzyl)pyridinium bromide (MP). This probe exhibited intense green emission, which was selectively quenched by the addition of ClO^- anions. The response of probe MP-ZIF-90 toward ClO^- was rapid (within 20 s) and sensitive, with a limit of detection (LOD) of 0.612 μM. Importantly, the utilization of the probe in the fluorescence imaging of ClO^- anions in the mitochondria of living cells and zebrafish was demonstrated.

1. Introduction

As essential organelles in eukaryotic cells, mitochondria are involved in many vital cellular processes and have been demonstrated to be the principal source of intracellular reactive oxygen species (ROS).[1–3] Among the various ROS, hypochlorite (ClO^-), generated by the oxidation of Cl^- with hydrogen peroxide (H_2O_2) catalyzed by mitochondrial myeloperoxidase (MPO), plays a crucial role in a variety of physiological processes, including maintaining intracellular oxidative balance, and defending against the invasion of some pathogens in the human immune system.[4,5] However, its abnormal expression would induce tissue damage and various diseases, such as rheumatoid arthritis, cardiovascular disease, arteriosclerosis, kidney disease, and even cancer. Therefore, it is desirable to develop methods to monitor the release of mitochondrial ClO^-.

To date, fluorescent probe technology has been regarded as one of the most efficient tools for biological analysis due to its real-time monitoring and non-invasive features.[6–10] Accordingly, a large number of molecular probes have been utilized to sense ClO^- primarily based on its highly oxidizing properties. However, many of them are limited by the complexity of the synthetic processes, non-specific targeting, poor water solubility, and high toxicity, which strongly hinder their application in biological systems (Table S1†).[11–16]

More recently, metal–organic frameworks (MOFs) with geometrically well-defined structures have attracted substantial attention in the fields of biomedicine and biosensors.[17–21] Besides, zeolitic imidazolate framework-90, derived from Zn^{2+} and an imidazole-2-carboxaldehyde (2-ICA) ligand, has been widely used in ATP imaging, owing to its distinct chemical stability and excellent biocompatibility, as well as mitochondria-targeting ability.[17] Moreover, the covalent functionalization of the free aldehyde groups in the ZIF-90 framework is easily achieved, supporting its role as a fluorometric sensor. Practically, the porous framework of ZIF-90-based probes increases the sensitivity and selectivity when compared with molecular probes. Nevertheless, to the best of our knowledge, fluorescent probes based on the ZIF-90 skeleton for ClO^- detection have not been reported.

Considering the abovementioned circumstances, we introduced a terminal benzylborate ester moiety as the recognition site for ClO^- on the pore surface of ZIF-90 *via* a post-synthetic method using 4-methyl-1-(4-(4,4,5,5-tetramethyl-1,3,2-dioxa-

[a]*College of Chemistry and Chemical Engineering, Henan Key Laboratory of Coal Green Conversion, Henan Polytechnic University, Jiaozuo 454000, P. R. China. E-mail: wuwn08@hpu.edu.cn, wangyuan08@hpu.edu.cn*
[b]*Key Laboratory of Chemo/Biosensing and Detection, College of Chemical and Materials Engineering, Xuchang University, Xuchang, 461000, P. R. China. E-mail: xuzhihong1980@xcu.edu.cn*
[c]*College of Chemistry, Zhengzhou University, Zhengzhou, 450052, P. R. China*
[d]*Department of Chemistry, College of Science King Saud University, Riyadh, 11451, Saudi Arabia*
[e]*Department of Chemistry, University of North Texas, Denton, 76203-5070, USA. E-mail: Shengqian.Ma@unt.edu*

†Electronic supplementary information (ESI) available. See DOI: https://doi.org/10.1039/d3dt00829k

‡These authors equally contributed to this work.

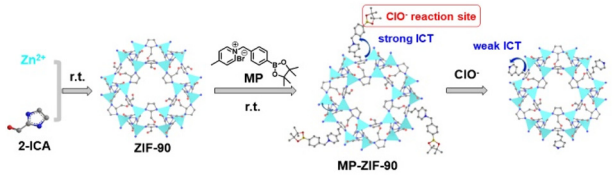

Scheme 1 Synthetic route of probe MP-ZIF-90 and its reaction mechanism with ClO^-.

borolan-2-yl)benzyl)pyridinium bromide (MP),[22] thereby fabricating a novel organic–inorganic hybrid probe MP-ZIF-90 (Scheme 1) for the sensitive detection of ClO^-. As expected, probe MP-ZIF-90 emitted a bright green light at 500 nm in a pure aqueous solution, owing to the strong intramolecular charge transfer (ICT) effect from ZIF-90 to pyridinium. The emission band of probe MP-ZIF-90 was totally and specifically quenched by ClO^-, due to the departure of the benzylborate ester group, which disrupted the ICT process. Finally, probe MP-ZIF-90 has been successfully implemented to probe endogenous or exogenous ClO^- levels in the mitochondria of cells and zebrafish.

2. Results and discussion

2.1 Synthesis and characterization of MP-ZIF-90

ZIF-90 was synthesized as reported in the literature,[17] and its free CHO group was modified by condensation with 4-methyl-1-(4-(4,4,5,5-tetramethyl-1,3,2-dioxaborolan-2-yl)benzyl)pyridinium bromide (MP) under the catalysis of piperidine at room temperature to generate the probe, designated as MP-ZIF-90. Compared with ZIF-90, MP-ZIF-90 displayed new peaks at 2992, 1522, 1097, and 857 cm^{-1} in the IR spectrum (Fig. 1), which were attributed to MP. However, the PXRD curves of both MP-ZIF-90 and ZIF-90 were consistent with that of the simulated crystal structure (Fig. 2), indicating that MP was reasonably well grafted inside the pore of ZIF-90 instead of the

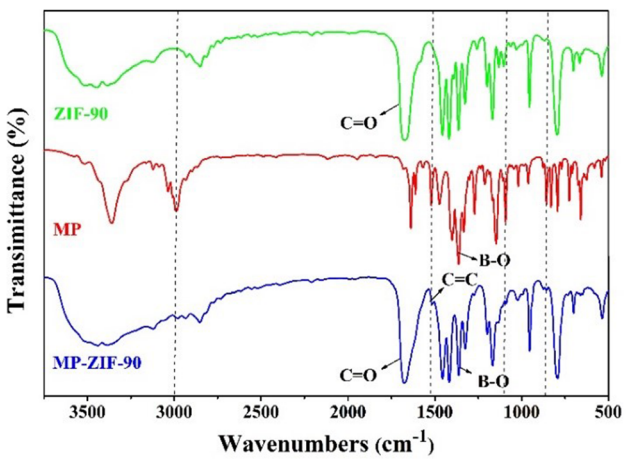

Fig. 1 IR spectra of ZIF-90, MP, and probe MP-ZIF-90.

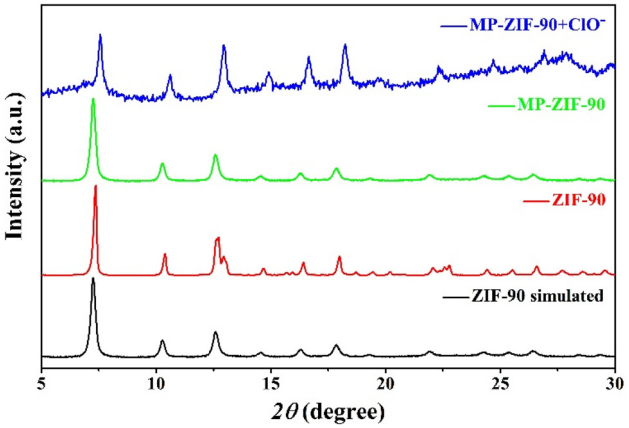

Fig. 2 PXRD spectra of ZIF-90, MP-ZIF-90, and MP-ZIF-90 + ClO^-.

surface. N_2 gas sorption measurements were carried out to further investigate the inner porosity difference between MP-ZIF-90 and ZIF-90. As shown in Fig. S1, ESI and Table S2,† the average pore diameter of MP-ZIF-90 (0.889 nm) was significantly decreased compared with that of ZIF-90 (4.077 nm) based on the BET surface area and nonlocal density functional theory (NLDFT) analyses, mainly because of the partial pore blockage induced by the modified MP moieties. In addition, the energy dispersive X-ray spectrum (EDS) revealed the existence of Br in the MP-ZIF-90 probe, which was encapsulated as a counter anion, while no distinct peaks of element B were found, probably due to its weak diffraction (Fig. 3).

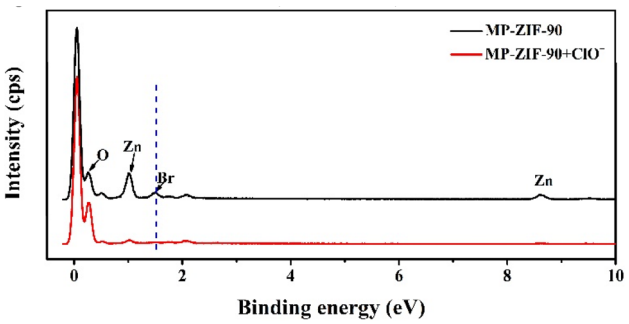

Fig. 3 EDS spectra of MP-ZIF-90 and MP-ZIF-90 + ClO^-.

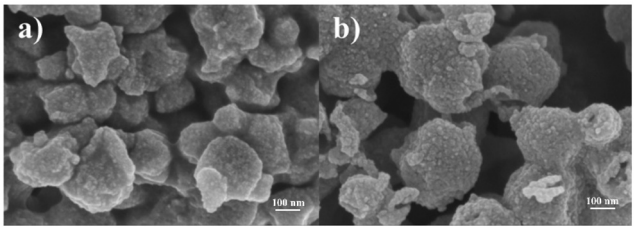

Fig. 4 SEM morphology of MP-ZIF-90 (a) and MP-ZIF-90 + ClO^- (b). Scale bar: 100 nm.

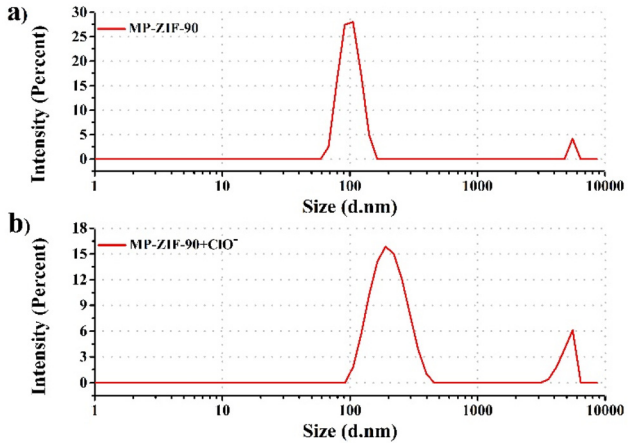

Fig. 5 DLS spectra of MP-ZIF-90 (a) and MP-ZIF-90 + ClO^- (b).

Furthermore, uniformly dispersed nanospherical particles of the MP-ZIF-90 probe were observed based on scanning electron microscopy (SEM), as shown in Fig. 4. The *Z*-average diameter was estimated at 398.7 nm *via* dynamic light scattering (DLS) analysis (Fig. 5). Taken together, the combined data support the successful incorporation of MP into the pore of ZIF-90 in the MP-ZIF-90 probe.

2.2 Fluorescent response of MP-ZIF-90 to ClO^-

The nanosized hybrid probe MP-ZIF-90 was well dispersed in water, so pure H_2O was selected as the test medium. As shown in Fig. 6b, the aqueous solution of probe MP-ZIF-90 (25 μg mL^{-1}) displayed an emission peak at 500 nm with excitation at 380 nm (Φ = 0.317, using fluorescein as a standard),[23] according to the intense green color of the solution under a 365 nm UV lamp. The emission was attributed to the ICT effect from ZIF-90 to grafted pyridinium. Upon the progressive addition of ClO^- up to 500 μM, the green fluorescence of the probe was gradually quenched in a dose-dependent manner, and the solution darkened under 365 nm irradiation. The fluorescence intensity at 500 nm (F_{500}) showed a good linearity with ClO^- concentration in the range of 60–100 μM (R^2 = 0.99332), indicating that probe MP-ZIF-90 could be potentially employed to quantitatively detect ClO^-. Accordingly, a limit of detection of 0.612 μM was obtained based on $3\delta/k$,[24–26] which was substantially lower than that of some molecular probes reported for detecting ClO^- (Table S1†), thereby demonstrating the high sensitivity of the fabricated probe for ClO^- detection.

The selectivity of the MP-ZIF-90 probe toward ClO^- was also pronounced. As shown in Fig. 6a, adding ClO^- (500 μM) to the probe solution (25 μg mL^{-1}) totally quenched the green fluorescence (Φ = 0.087). By contrast, except for $ONOO^-$ and $^{\bullet}OH$, which reduced the fluorescence of the MP-ZIF-90 probe to 45% and 70%, respectively, other anions (F^-, Cl^-, Br^-, I^-, ClO_4^-, CN^-, $H_2PO_4^-$, HPO_4^-, HSO_3^-, HSO_4^-, OAc^-, PO_4^{3-}, PPi, S^{2-}, SO_4^{2-}, and SO_3^{2-}), amino acids (Met, Pro, His, Cys, Hcy, and GSH), and ROS (H_2O_2, $ONOO^-$, $^1O_2$, $^{\bullet}OH$, NO, and ROO^-) at the same concentration as ClO^- induced negligible changes in the fluorescent spectrum of the probe, and the detection of ClO^- using the MP-ZIF-90 probe was still effective despite the co-existence of the competitive species mentioned above (Fig. S2, ESI†). All evidence suggests that our probe possesses high selectivity toward ClO^- compared with other analytes.

Importantly, we also investigated the time course effect of the fluorescence intensity of probe MP-ZIF-90 with and without ClO^-. As illustrated in Fig. S3, ESI,† the F_{500} value of free MP-ZIF-90 remained relatively stable in pure H_2O and decreased upon the addition of ClO^- (within 20 s), revealing the fast response of MP-ZIF-90 toward ClO^-. This feature was absent in some reported mitochondria-targeting fluorescent ClO^- probes (Table S1†). In addition, the effect of pH on the detection of ClO^- was also evaluated. The results indicate that the reaction between MP-ZIF-90 and ClO^- occurred in the pH range of 4.0–11.0 (Fig. S4, ESI†), which suggests that MP-ZIF-90 facilitates the rapid detection of ClO^- under physiological conditions.

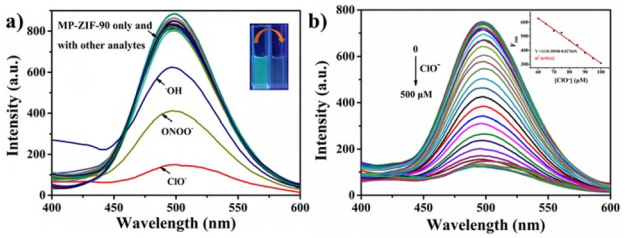

Fig. 6 (a) Fluorescence spectra of probe MP-ZIF-90 (25 μg mL^{-1}) in pure H_2O with 500 μM of anions (F^-, Cl^-, Br^-, I^-, ClO_4^-, CN^-, $H_2PO_4^-$, HPO_4^-, HSO_3^-, HSO_4^-, OAc^-, PO_4^{3-}, PPi, S^{2-}, SO_4^{2-}, and SO_3^{2-}), amino acids (Met, Pro, His, Cys, Hcy, and GSH), and ROS (H_2O_2, $ONOO^-$, $^1O_2$, $^{\bullet}OH$, NO, and ROO^-) and blank. (b) Fluorescence spectra of probe MP-ZIF-90 (25 μg mL^{-1}) upon the addition of ClO^- (0–500 μM) in pure H_2O. Inset: (a) the solution color change of MP-ZIF-90 with ClO^- under a 365 nm UV lamp; (b) the F_{500} of MP-ZIF-90 as a function of ClO^- concentration with a linear relationship. The excitation wavelength was 380 nm.

2.3 Sensing mechanism

Since benzylborate ester is a frequently used recognition site for ClO^- in molecular probe design, we speculated on the occurrence of a similar elimination reaction in the case of the reaction between probe MP-ZIF-90 and ClO^-, which was strongly supported by EDS analysis. Based on the results shown in Fig. 3, the weight percentage of Br in probe MP-ZIF-90 decreased from 2.39% to 0.42% in the presence of ClO^-, clearly indicating the release of the benzylborate ester group of MP-ZIF-90 following the addition of ClO^-. In addition, the PXRD spectrum of MP-ZIF-90 with ClO^- was similar to that of MP-ZIF-90 (Fig. 2), and the *Z*-average particle size of MP-ZIF-90 with ClO^- was 393.9 nm (Fig. 4), which was comparable to the value of MP-ZIF-90 (398.7 nm). Nevertheless, the surface of MP-ZIF-90 particles became rougher after treatment with ClO^- based on SEM morphological analysis, which might be induced by the reaction between MP-ZIF-90 and ClO^- as illustrated in Scheme 1.

2.4 Fluorescence imaging of MP-ZIF-90 in living cells

To further investigate the *in vivo* application of the MP-ZIF-90 probe, its biocompatibility was established in HeLa cells based on the MTT assay (Fig. S5, ESI†).[27] The results show that each cell viability was greater than 90% under the MP-ZIF-90 staining concentrations (0–100 μg mL^{-1}), revealing the low cytotoxicity of our probe during bioimaging applications.

No fluorescence signals were detected in three kinds of cells (HeLa, HepG2, and RAW 264.7 cells) in the absence of probe MP-ZIF-90, showing minimal biological fluorescent background (Fig. 7 and Fig. S6, S7, ESI†). After treatment with MP-ZIF-90 (25 μg mL^{-1}) for 30 min, the cells displayed a light fluorescence signal in the green channel, which was seriously weakened when exposed to ClO^- (500 μM) for another 30 min. A similar quenching phenomenon was observed when the cells were pre-incubated with lipopolysaccharide (LPS, an endogenous ClO^- stimulator, 5 μg mL^{-1}) for 30 min before treatment with MP-ZIF-90 for another 30 min. However, the light green fluorescence persisted when the cells were pre-treated with LPS (5 μg mL^{-1}) and *N*-acetyl-L-cysteine (NAC, 500 μM, an endogenous ClO^- inhibitor), and then incubated with probe MP-ZIF-90. All the abovementioned findings confirm that probe MP-ZIF-90 is capable of imaging exogenous and endogenous ClO^- in living cells.

To assess the subcellular localization of probe MP-ZIF-90, a co-staining experiment with HeLa cells was carried out. As shown in Fig. 8, the green fluorescence of probe MP-ZIF-90 merged well with the red fluorescence of Mito-Tracker Red (a commercial mitochondrial tracker). The overlap coefficient was estimated to be 0.89, demonstrating the strong mitochondria-targeting ability of probe MP-ZIF-90.

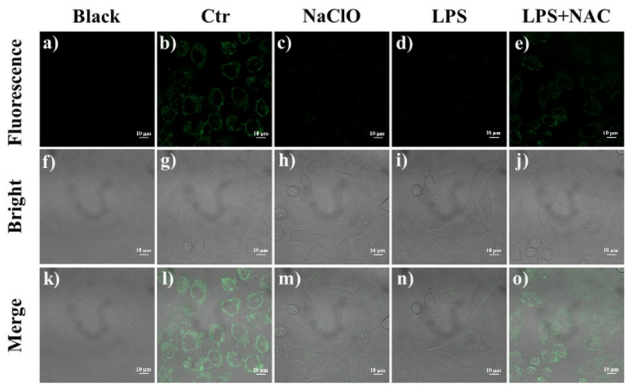

Fig. 7 Fluorescence images of probe MP-ZIF-90 (25 μg mL^{-1}) in HeLa cells: (a–e) green channel; (f–j) bright field; (k–o) the merged images of (a–e) and (f–j); (a, f and k) images of HeLa cells only for 30 min at 37 °C; (b, g and l) images of HeLa cells incubated with MP-ZIF-90 (25 μg mL^{-1}) for 30 min at 37 °C; (c, h and m) images of MP-ZIF-90-loaded (25 μg mL^{-1}) HeLa cells incubated with NaClO (500 μM) for 30 min at 37 °C; (d, i and n) images of MP-ZIF-90-loaded (25 μg mL^{-1}) HeLa cells pre-treated with LPS (5 μg mL^{-1}) for 30 min at 37 °C; (e, j and o) images of MP-ZIF-90-loaded (25 μg mL^{-1}) HeLa cells pre-treated with LPS (5 μg mL^{-1}) and NAC (500 μM) for 30 min at 37 °C. Scale bar: 10 μm.

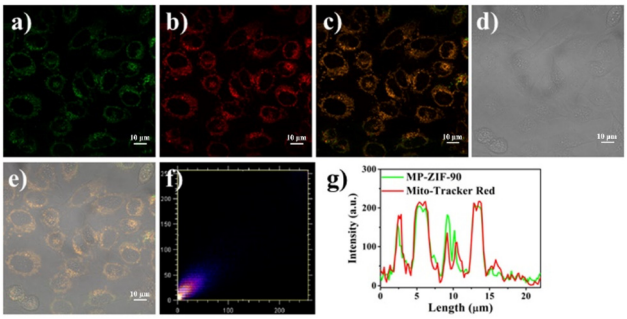

Fig. 8 Fluorescence images of HeLa cells stained with 25 μg mL^{-1} of probe MP-ZIF-90 and Mito-Tracker Red: (a) green channel; (b) red channel (mitochondria staining); (c) an overlay of red and green channels; (d) bright field; (e) an overlay of red and green channels and bright field; (f) an intensity scatter plot of green and red channels; (g) intensity profile of the linear region of interest across the HeLa cells co-stained with Mito-Tracker Red and the green channel of MP-ZIF-90. Scale bar: 10 μm.

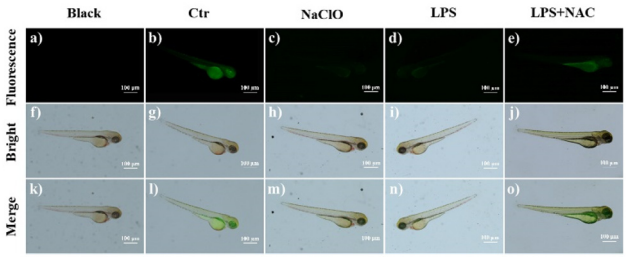

Fig. 9 Fluorescence images of probe MP-ZIF-90 (25 μg mL^{-1}) in zebrafish: (a–e) green channel; (f–j) bright field; (k–o) the merged images of (a–e) and (f–j); (a, f and k) images of zebrafish only for 30 min at 28 °C; (b, g and l) images of zebrafish incubated with MP-ZIF-90 (25 μg mL^{-1}) for 30 min at 28 °C; (c, h and m) images of MP-ZIF-90-loaded (25 μg mL^{-1}) zebrafish incubated with NaClO (500 μM) for 30 min at 28 °C; (d, i and n) images of MP-ZIF-90-loaded (25 μg mL^{-1}) zebrafish pre-treated with LPS (5 μg mL^{-1}) for 30 min at 28 °C; (e, j and o) images of MP-ZIF-90-loaded (25 μg mL^{-1}) zebrafish pre-treated with LPS (5 μg mL^{-1}) and NAC (500 μM) for 30 min at 28 °C. Scale bar: 100 μm.

Accordingly, this probe has potential for applications in determining mitochondrial ClO^- in living cells.

2.5 Fluorescence imaging of MP-ZIF-90 in zebrafish

Based on the promising performance of the MP-ZIF-90 probe in cellular imaging, we explored its ability for monitoring ClO^- in zebrafish. The strong green fluorescence could be observed when the zebrafish were cultured with only MP-ZIF-90 (25 μg mL^{-1}), or pre-treated with LPS and NAC, followed by MP-ZIF-90 for 30 min (Fig. 9). In contrast, the zebrafish treated with MP-ZIF-90 and then ClO^-, or pre-treated with LPS, followed by MP-ZIF-90, manifested weak green fluorescence, in accordance with the results derived from cellular imaging, suggesting that the MP-ZIF-90 probe can be used to detect exogenous/endogenous ClO^- in living animals.

3. Conclusion

In summary, we developed a hybrid probe MP-ZIF-90 based on ZIF-90 *via* a post-synthetic approach, whose structure was fully characterized by a wide range of spectroscopic, microscopic and surface science techniques including PXRD, IR, SEM, EDS, DLS, BET, and NLDFT. The probe exhibited excellent dispersion in pure aqueous solution with an intense green emission, which was turned off in response to ClO^- in a rapid, selective and sensitive manner. The sensing mechanism suggested a ClO^--induced elimination of the terminal benzylborate ester group. Importantly, the fabricated probe was used to monitor mitochondrial ClO^- in living cells and zebrafish.

Author contributions

L. Z. contributed to data curation and writing – review and editing. X. C. contributed to data curation and writing – review and editing. W.-N. W. contribute to validation. X.-L. Z. contributed to conceptualization, software, and resources. Y.-C. F. contributed to methodology. Y. W. contributed to writing – original draft preparation, and funding acquisition. Z.-H. X. contributed to supervision and project administration. A. N. contributed to funding acquisition. A. M. A. contributed to reviewing. S. Q. M. contributed to methodology.

Conflicts of interest

There are no conflicts to declare.

Acknowledgements

This work was supported in part by the National Natural Science Foundation of China (no. 21907023 and 21001040), the Joint Program for Fostering Talents of the National Natural Science Foundation of China and Henan Province (no. U1304202), the Science and Technology Department of Henan Province (no. 212102210033, 222300420523, and 212102210646), the Key Program of Xuchang University (no. 2022CXTD001), and the Researcher Supporting Program number (RSP2023R79) at King Saud University, Riyadh, Saudi Arabia. Partial support from the Robert A. Welch Foundation (B-0027) is also acknowledged (S. M.).

Notes and references

1 K. L. Ma, G. Chen, W. H. Li, O. Kepp, Y. S. Zhu and Q. Chen, *Front. Cell Dev. Biol.*, 2020, **8**, 467.
2 P. Hernansanz-Agustín and J. A. Enríquez, *Antioxidants*, 2021, **10**, 415.
3 B. Y. Zhang, C. Y. Pan, C. Feng, C. Q. Yan, Y. J. Yu, Z. L. Chen, C. J. Guo and X. X. Wang, *Redox Rep.*, 2022, **27**, 45–52.
4 W. J. Liu, Y. Y. Wang, N. Wu, W. Feng, Z. X. Li, L. H. Wei and M. M. Yu, *Spectrochim. Acta, Part A*, 2020, **240**, 118564.
5 N. S. Zhu, X. L. Guo, Y. L. Chang, Z. Shi, L. Y. Jin and S. H. Feng, *Dyes Pigm.*, 2022, **201**, 110227.
6 W. Y. Xu, Z. Z. Shou, C. Tang, C. Zhang, Y. H. Chen and Y. Liang, *Org. Biomol. Chem.*, 2022, **20**, 5953–5957.
7 A. Tariq, U. Garnier, R. Ghasemi, J. P. Lefevre, C. Mongin, A. Brosseau, J. F. Audibert, R. Pansu, A. Dauzères and I. Leray, *J. Photochem. Photobiol., A*, 2022, **432**, 114035.
8 Y. L. Zheng, X. C. Li, W. Tang, L. Xie, F. Dai and B. Zhou, *Sens. Actuators, B*, 2022, **368**, 132169.
9 M. M. Fortibui, D. W. Yoon, J. Y. Lim, S. Lee, M. Choi, J. S. Heo, J. Kim and J. Kim, *Dalton Trans.*, 2021, **50**, 2545–2554.
10 G. S. Malankar, D. S. Shelar, M. Manikandan, M. Patra, R. J. Butcher and S. T. Manjare, *Dalton Trans.*, 2022, **51**, 10069–10076.
11 N. An, D. Wang, H. Zhao and Y. L. Gao, A spectroscopic probe for hypochlorous acid detection, *Spectrochim. Acta, Part A*, 2022, **267**, 120529.
12 W. D. Hu, M. Zhao, K. Y. Gu, L. W. Xie, M. Liu and D. Q. Lu, *RSC Adv.*, 2022, **12**, 777.
13 X. Tang, Z. Zhu, R. J. Liu and Y. Tang, *Spectrochim. Acta, Part A*, 2019, **219**, 576–581.
14 H. F. Li, Y. Miao, Z. X. Liu, X. Wu, C. X. Piao and X. Zhou, *Dyes Pigm.*, 2020, **176**, 108192.
15 G. Li, D. D. Ji, S. M. Zhang, J. M. Li, C. Li and R. Z. Qiao, *Sens. Actuators B*, 2017, **252**, 127–133.
16 Q. Yang, X. Zhong, Y. Chen, J. Yang, C. Jin and Y. Jiang, *Analyst*, 2020, **145**, 3100–3105.
17 J. J. Deng, K. Wang, M. Wang, P. Yu and L. Q. Mao, *J. Am. Chem. Soc.*, 2017, **139**, 5877–5882.
18 J. Chen, Y. Chen, S. Y. Li, J. Yang, J. B. Dong and X. Q. Lu, *Carbon*, 2022, **199**, 110–118.
19 W. A. El-Fattah, E. S. Al-Farraj, N. B. Hamadi, A. Alharbi and A. Shahat, *ACS Omega*, 2022, **7**, 17483–17491.
20 Y. N. Zeng, H. Q. Zheng, X. H. He, G. J. Cao, B. Wang, K. C. Wu and Z. J. Lin, *Dalton Trans.*, 2020, **49**, 9680–9687.
21 Y. X. Ye, L. W. Zhao, S. G. Hu, A. J. Liang, Y. S. Li, Q. X. Zhuang, G. R. Tao and J. L. Gu, *Dalton Trans.*, 2019, **48**, 2617–2625.
22 Y. Ni, H. Liu, D. Dai, X. Q. Mu, J. Xu and S. J. Shao, *Anal. Chem.*, 2018, **90**, 10152–10158.
23 Y. B. Gan, G. X. Yin, T. Yu, Y. Y. Zhang, H. T. Li and P. Yin, *Talanta*, 2020, **210**, 120612.
24 X. Zhong, Q. Yang, Y. Chen, Y. Jiang and Z. Dai, *J. Mater. Chem. B*, 2020, **8**, 7375–7381.
25 T. R. Wang, X. F. Zhang, X. Q. Huang, X. Q. Cao and S. L. Shen, *Spectrochim. Acta, Part A*, 2021, **247**, 119115.
26 F. F. Guo, W. N. Wu, X. L. Zhao, Y. Wang, Y. C. Fan, C. X. Zhang and Z. H. Xu, *Spectrochim. Acta, Part A*, 2022, **264**, 120270.
27 P. Kumar, N. Kaur, P. Tiwari, A. K. Gupta and S. M. Mobin, *ACS Mater. Lett.*, 2023, **5**, 1100–1108.

